Journal of Power Sources 189 (2009) 721–725

Contents lists available at ScienceDirect

Journal of Power Sources

journal homepage: www.elsevier.com/locate/jpowsour

Short communication

Electrochemical performance and capacity fading reason of $LiMn_2O_4$/graphite batteries stored at room temperature

Yunjian Liu, Xinhai Li*, Huajun Guo, Zhixing Wang, Qiyang Hu, Wenjie Peng, Yong Yang

School of Metallurgical Science and Engineering, Central South University, Changsha 410083, China

ARTICLE INFO

Article history:
Received 27 June 2008
Received in revised form 14 August 2008
Accepted 15 August 2008
Available online 27 August 2008

Keywords:
$LiMn_2O_4$
Electrochemical performance
Capacity fading reason
Storage performance
XPS

ABSTRACT

This paper describes the fabrication of $LiMn_2O_4$/graphite batteries and their performance after storage at room temperature. The discharge capacity and cyclic performance of the batteries were investigated. Compared with the batteries without storage, those after storage show better cyclic performance with a capacity retention ratio of 94.2% after 100 cycles, yet deliver lower capacity. The ratio of capacity recovery after storage at room temperature for a month is 96.3%. The reason for the capacity fading and better cyclic performance was studied with XRD, SEM, EDS, XPS, cyclic voltammograms and AC impedance. It is found that the lattice parameter of $LiMn_2O_4$ shrinks after storage. Mn is dissolved into the electrolyte and deposited on the anode, and the electrode surface is covered by MnO_2. The migration resistance of $LiMn_2O_4$/electrolyte is increased from 20.28 to 53.31 Ω after storage due to the covered MnO_2. But the deposited MnO_2 also separates the $LiMn_2O_4$ from electrolyte, which can improve the cyclic performance.

1. Introduction

In the near future, there are plenty of opportunities for the electric vehicle (EV) and hybrid electric vehicle (HEV) with the rechargeable battery as power source to substitute the traditional vehicle. The requests of the rechargeable lithium ion battery are nothing more than low cost, safety, high energy density and green. Among all candidate cathode materials, $LiMn_2O_4$ is proposed to satisfy the field-use requirements and becomes the promising cathode material for commercial usage. However, the cells used spinel $LiMn_2O_4$ as a cathode material have been known to cause severe capacity fading on charge–discharge cycling or storage, especially at high temperature [1–4].

The mechanism of the capacity fading during charge–discharge cycling has not been completely clarified, although some factors concerned have been discussed: (i) electrochemical reactions of electrolyte solution at high voltage (above 4.0 V); (ii) irreversible phase and structure transition [5–7] (i.e. Jahn-Teller distortion); (iii) Mn dissolution of spinel $LiMn_2O_4$ cathode into the electrolyte according to the disproportional reaction: $2Mn^{3+} \rightarrow Mn^{4+} + Mn^{2+}$ [8–11].

Many research groups have attempted to stabilize the structure of $LiMn_2O_4$ powders during cycling by substituting a small fraction of the manganese-ions with several divalent or trivalent metal ions (M = Al, Se, Mg, Zn, Co, Ti, Ni, Fe, Cr) [12–21] in the 16 d sites. On the other hand, an appropriate method to reduce capacity fades of $LiMn_2O_4$ is surface coating of the spinel to avoid Mn dissolution [22–23]. And they have achieved good results. The cycling performance has been improved effectively.

During the fabrication, sale and use of the Li-ion battery, the battery will be stored for several months. The ratio of spinel battery capacity recovery after storage is very important to practical use. Yamane et al. [24], Takahashi et al. [25] and Saitoh et al. [26] studied the storage performance of $LiMn_2O_4$, and concluded that the capacity fading was because of the poor conduction between the active material and collector.

In this study, the storage and charge–discharge cyclic performance of Li-ion batteries were studied by using commercially available $LiMn_2O_4$ as cathode material and graphite as anode. Structure and morphology of the cathode electrode after storage were characterized by XRD and SEM technique, respectively. XPS, cyclic voltammograms and AC impedance were used to analyse the surface state change of $LiMn_2O_4$ electrode after storage. And a new reason of capacity fading after storage was given.

2. Experimental

2.1. Battery fabrication

The 204468 type Li-ion batteries use $LiMn_2O_4$ as the cathode and graphite as anode. The electrolyte was 1 M $LiPF_6$ in mixture of

* Corresponding author. Tel.: +86 731 8836633.
E-mail address: lyjian122331@yahoo.com.cn (L. Xinhai).

0378-7753/$ – see front matter © 2008 Elsevier B.V. All rights reserved.
doi:10.1016/j.jpowsour.2008.08.044

ethylene carbonate (EC)/diethyl carbonate (DEC)/dimethyl carbonate (DMC) 1:1:1 by volume.

2.2. Electrochemical performance test

The capacity test of batteries were charged at 1/3*C* rate to 4.2 V and then discharged at 1/3*C* rate to 3.0 V at 25 °C. For the cycling test, current for charge–discharge were held at 0.5*C*.

Electrochemical impedance spectroscopy (EIS) and cyclic voltammograms (CV) measurements of the cell were carried out using CHI660A (Chenghua, Shanghai). The amplitude of the AC signal was 5 mV over the frequency range between 100 kHz and 0.01 Hz. The sweep rate of CV was 0.1 mV s^{-1} over a potential of 2.5–4.5 V.

2.3. Storage performance test

The batteries were charged to half charged state, and then stored at room temperature for 28 days. After storing, the batteries were initially discharged to 3.0 V at 0.2*C* rate, and then charged to 4.2 V and again discharged to 3.0 V at 0.2*C* rate to measure their capacity.

2.4. Structure and surface analysis

For evaluating the cell materials after a charge–discharge cycling and storing, the cathode and anode electrodes were collected by disassembling the tested cells in argon-filled glove box. The cathode and anode materials were washed with EC + DEC mixed solution to remove the electrolyte salt.

The crystal structure of the cathode and anode were characterized by X-ray diffraction with Cu Kα radiation monochromator at a step width of 0.02°.The morphology was measured by scanning electron microscope (JEOL, JSM-5600LV) with an accelerating voltage of 20 kV. The elements on the surface of graphite electrode were identified by energy-dispersive X-ray spectroscopy (EDS).

The surface analysis of $LiMn_2O_4$ electrode materials with discharge state, were carried out with ESCA-5700ci XPS (Physical Electronics Co.).

3. Results and discussion

The results of discharge capacity before and after storage are shown in Fig. 1. The discharge capacities of $LiMn_2O_4$/graphite before and after storage are 106.8 and 102.8 mAh g^{-1}, respectively. The ratio of capacity recovery after storage is 96.3%. That is to say

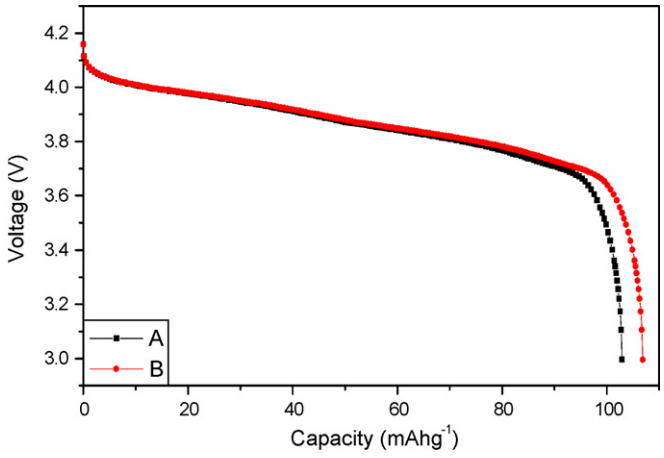

Fig. 1. Discharge curve of $LiMn_2O_4$ electrode: (A) after storage and (B) before storage.

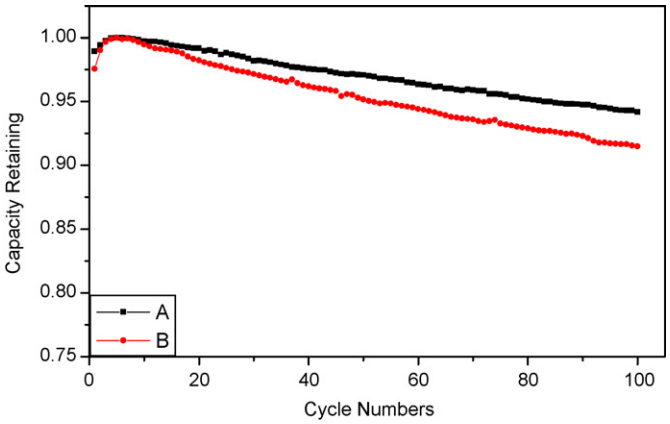

Fig. 2. The cycle performance of battery at room temperature: (A) after storage and (B) before storage.

that 3.7% capacity of battery is lost during the storage with half charged at room temperature for 28 days without cycling. It is well known that the capacity fading during storage is commonly linked to the Mn dissolution [9,10].

Fig. 2 shows the discharge capacity profiles of $LiMn_2O_4$/graphite battery before and after storage according to cycle number at a current density of 0.5*C* rate between 3.0 and 4.2 V. As shown in Fig. 2, the $LiMn_2O_4$ battery after storage shows better cycling performance during 100 cycles with the retention of 94.2%, and the $LiMn_2O_4$ battery without storage shows the retention of 91.4%. The results indicate that the cycling performance of spinel battery is improved after storage. Fig. 2 also shows that the cyclic performances of $LiMn_2O_4$ battery were improved with the cycle proceeding. From the sixth cycle, the capacity retentions of $LiMn_2O_4$ batteries before and after storage after initial 47 cycles are 5.16 and 3.19%, and that of the latter 47 cycles are 3.37 and 2.66%, respectively. This can be concluded that the amount of Li^+ inserting the $Li_xMn_2O_4$ is low because of the decreased discharge capacity, which results in higher value of Mn in the $Li_xMn_2O_4$ and minishing the Li^+ concentration in the vicinity of the material surface. So the Jahn-Teller distortion is restrained and results in better cyclic performance.

Fig. 3 shows the change of surface morphology for $LiMn_2O_4$ after storage. Compared with Fig. 3(a), the surface of $LiMn_2O_4$ shown in Fig. 3(b) is eroded badly by electrolyte during storage. The SEM images also indicate that the $LiMn_2O_4$ electrode reacts with electrolyte and results in Mn dissolution during the storage.

Fig. 4(a) shows XRD patterns of $LiMn_2O_4$ electrode. All the peaks in the XRD patterns of the $LiMn_2O_4$ electrode can be indexed as the spinel phase (JCPDS: 35-0782) except the characteristic peak of graphite, indicating that the $LiMn_2O_4$ retains spinel structure after storage.

Fig. 4(b) shows the magnified patterns at $2\theta = 35.5–40°$. Diffraction peaks of $LiMn_2O_4$ shift to higher angle after storage, indicating the shrinkage of crystal lattice. The lattice parameters of $LiMn_2O_4$ before and after storage are 8.2395 and 8.2223 Å, respectively. The result is in agreement with the X-ray diffraction pattern. The intensity of all peaks in the XRD patterns of the $LiMn_2O_4$ electrode were depressed after storage. The full width of the half maximum intensity (FWHM) of the (3 1 1) peak before and after storage is 0.26 and 0.28°, respectively. The result indicates that the crystallinity of the spinel decreased after storage.

Fig. 5 shows the EDS of anode before and after storage. In Fig. 5(a), no other elements except for C and O are detected from the surface of anode. But in Fig. 5(b), F, P and Mn are detected from the anode. Mn is from the dissolution of $LiMn_2O_4$. This result also

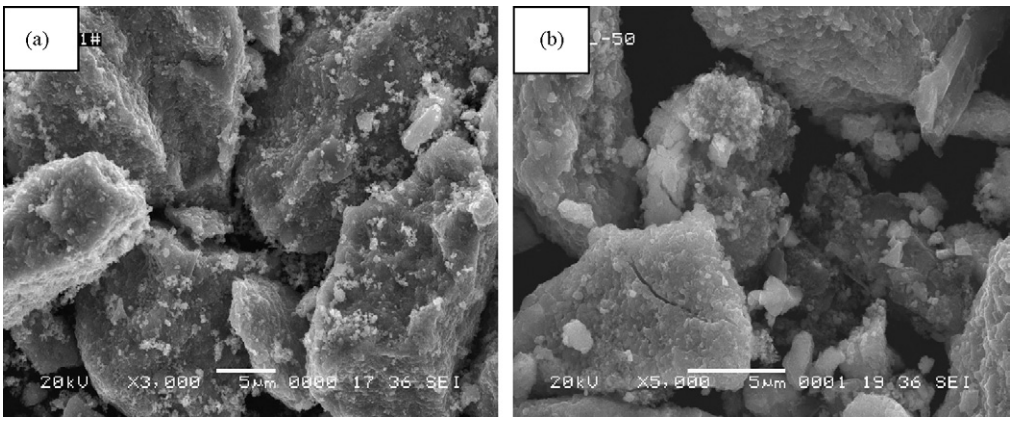

Fig. 3. SEM of $LiMn_2O_4$ electrode: (a) before storage and (b) after storage.

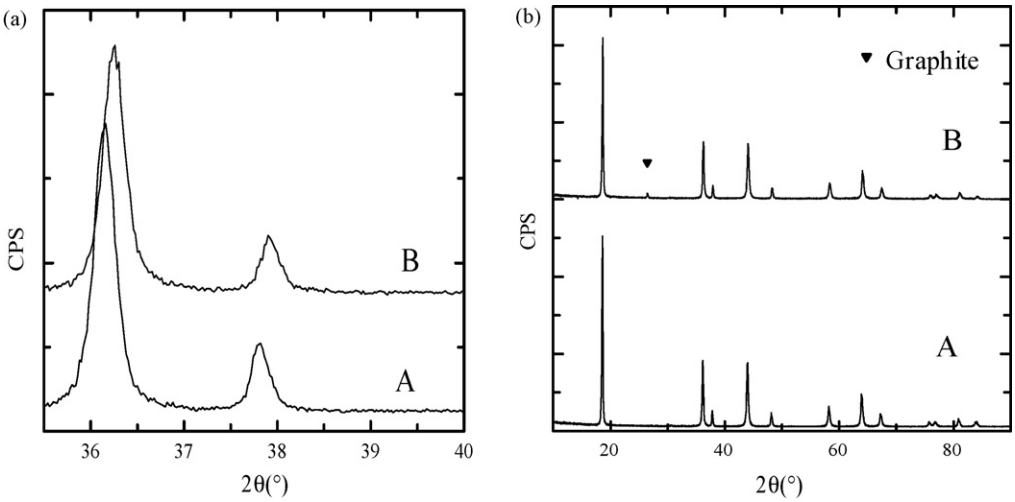

Fig. 4. XRD patterns of $LiMn_2O_4$ electrode: (A) before storage and (B) after storage.

validates that the Mn of $LiMn_2O_4$ is dissolved into the electrolyte and deposited on the anode electrode.

The dissolution of Mn is generally attributed to the existence of HF, which is easily formed in the case of using $LiPF_6$ as the electrolyte salt. The correlation of HF formation and Mn dissolution was experimentally reported [2]. $LiPF_6$ itself contains a small amount of HF during the manufacturing process, and the salt can easily react with water to form HF. Thus HF unavoidably exists

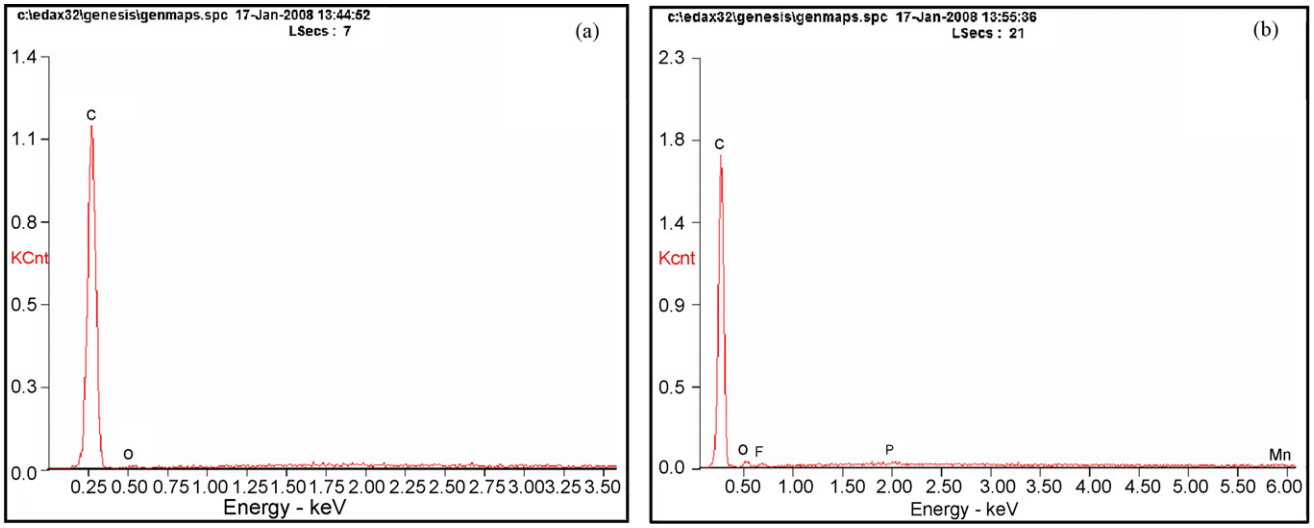

Fig. 5. EDS of the anode: (a) before storage and (b) after storage.

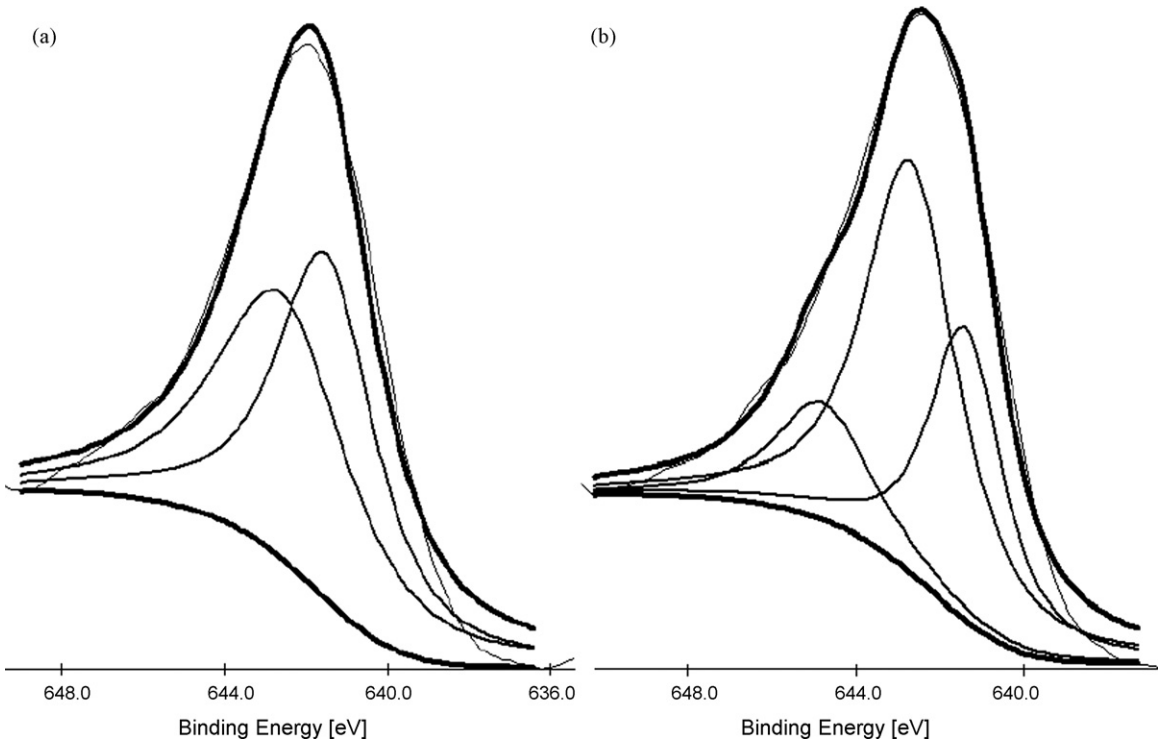

Fig. 6. XPS of $LiMn_2O_4$ electrode: (a) before storage and (b) after storage.

with very low concentration in the electrolyte, as shown in Li's paper [27].

The combination of HF–H_2O in the presence of air is known to react on the $LiMn_2O_4$ in an aqueous medium, according to the following equation [28]:

$$2LiMn_2O_4 + 4H^+ \rightarrow 3\lambda\text{–}MnO_2(s) + Mn^{2+}(l) + 2Li^+(l) + 2H_2O \quad (1)$$

MnO_2 is vice production of the Mn dissolution according the Eq. (1). The solid state MnO_2 should be deposited on the surface of $LiMn_2O_4$ electrode, and separates the $LiMn_2O_4$ electrode from the electrolyte. So it will be good to the electrochemical performance.

The Mn^{2+} is reduced and deposited on the anode surface, according to the following equation:

$$Mn^{2+} + 2e^- \rightarrow Mn \quad (2)$$

Fig. 6 shows the XPS results of the spinel $LiMn_2O_4$ electrode before and after storage. The observed binding energies of the Mn $2p_{3/2}$ are 642 and 642.4 eV, respectively. The results were fitted by XPS Peaking Fitting 4.1 software. In Fig. 6(a), it is divided into two peaks. One peak at binding energy situates at 642.6 eV, which is same with that observed in MnO_2 sample (642.6 eV). The other peak at binding energy situates at 641.51 eV, which is similar to the one observed in Mn_2O_3. From the ratio of the area for the first peak to that for the second peak, the contents of Mn^{3+} and Mn^{4+} are calculated to be 49.6 and 50.4%, respectively.

In Fig. 6(b), it is divided into three peaks. The first peak at binding energy situates at 641.4 eV, which is similar to the one observed in Mn_2O_3. The second one at binding energy situates at 642.7 eV, which is close to the one observed in MnO_2 sample (642.6 eV). The third one peak at binding energy situates at 644.8 eV, which may be the shaking up peak of Mn^{4+}. From the ratio of the area for first peak to that for the second one, the contents of Mn^{3+} and Mn^{4+} are calculated as 32.8 and 61.2%, respectively.

From the above results, we can conclude that the surface of $LiMn_2O_4$ is covered by MnO_2, which is from the Mn dissolution during storage. This conclusion is good with the Eq. (1). MnO_2 covered on the surface of $LiMn_2O_4$ can separate the contact of $LiMn_2O_4$ electrode/electrolyte interface and therefore improve the cyclic performance of $LiMn_2O_4$ battery. But the efficiency of $LiMn_2O_4$ electrode covered by MnO_2 is not clear.

Fig. 7 shows the cyclic voltammograms of $LiMn_2O_4$ cathode electrode measured with the potential range between 2.5 and 4.5 V versus Li/Li^+ at a sweep rate of 0.1 mV s^{-1} at room temperature. The CV curves of pristine and the stored $LiMn_2O_4$ electrode show two pairs of peak reflecting the typical oxidation processes of $LiMn_2O_4$ in 4.05 and 4.15 V (versus Li/Li^+) and de-oxidation processes in the 3.95 and 4.05 V, respectively, which involves phase transitions [29]. There is another pair of peak at 3.1 and 2.8 V. It is generally accepted

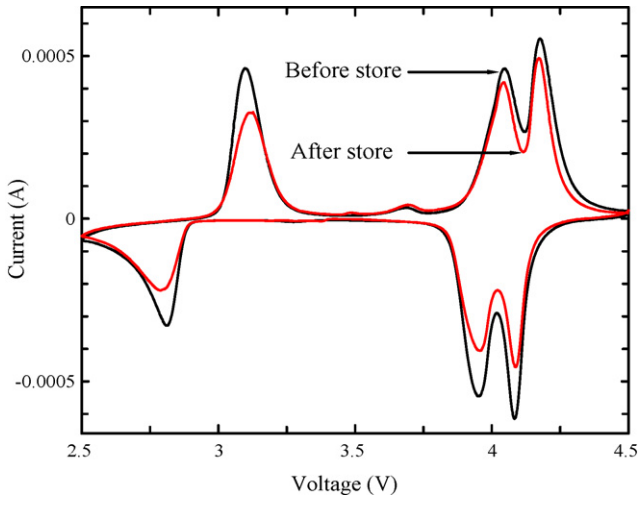

Fig. 7. Cyclic voltammogram curves of cathode electrode.

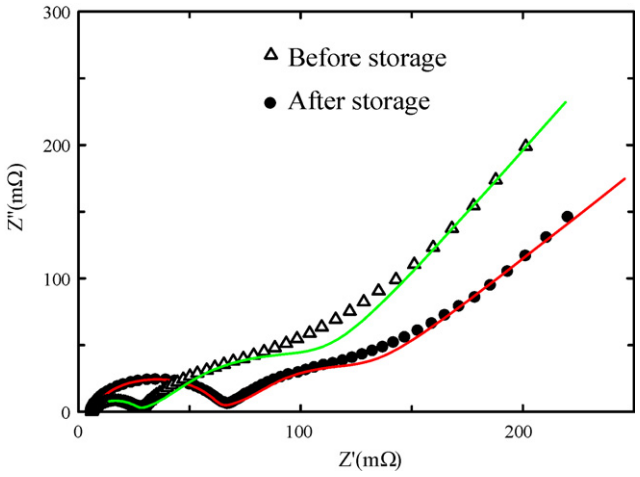

Fig. 8. AC impedance of $LiMn_2O_4$ electrode.

Table 1
Impedance parameters of equipment circuit

$LiMn_2O_4$ state	R_s (Ω)	R_f (Ω)	R_{ct} (Ω)
Before storage	5.01	20.28	37.4
After storage	5.81	53.31	25.52

that the electrode process around 3 V reflects a cubic-to-tetragonal phase transition as x in $Li_xMn_2O_4$ increases from 1 to 2 [30]. And there is another peak at 3.7 V during the oxide process, which is still unknown at present. The redox current for $LiMn_2O_4$ after storage (0.49 mA) is smaller than that for pristine $LiMn_2O_4$ (0.55 mA). These results indicate that the electrical conductivity of the $LiMn_2O_4$ electrode after storage is decreased.

To compare the surface state of $LiMn_2O_4$ before and after storage in more detail, AC impedance measurement was carried out using three-electrode configuration. In Fig. 8, the impedance spectra of $LiMn_2O_4$ before and after storage are combinations of two depressed semicircles in high frequency region and a straight line in low frequency region. An intercept at the Z_{real} axis in high frequency region corresponds to the ohmic resistance (R_s). The depressed semicircle in the high frequency range is related to the Li-ion migration resistance (R_f) through the SEI film formed on the cathode surface. The second semicircle in the middle frequency range indicates the charge transfer resistance (R_{ct}). The inclined line in the lower frequency represents the Warburg impedance (W), which is associated with lithium-ion diffusion in the $LiMn_2O_4$ particles.

The parameters of impedance spectra in Fig. 8 were simulated by Zview 2.0. The parameter results are listed in Table 1. The simulation results show that the Li-ion migration resistance is increased from 20.28 to 53.31 Ω after storage, which may be because of the MnO_2 film. And the total resistance is increased from 62.69 to 84.64 Ω. It is obvious that the ohmic and migration resistances produced by the stored $LiMn_2O_4$ electrode exceed the pristine ones.

So we just conclude that the capacity loss is not only because of the Mn dissolution, but also because of the increased Li-ion migration resistance and high cell polarization, leading an incomplete charging. According to Eq. (1), it can be concluded that the increase of resistance could be attributed to the deposited MnO_2.

4. Conclusions

In this paper, the $LiMn_2O_4$/graphite battery was fabricated and its storage performance was studied. 96.3% of capacity is recovered after storage with half charged state at room temperature for 28 days. Compared with the batteries without storage, those after storage show better cyclic performance with a capacity retention ratio of 94.2% after 100 cycles. It is found that the lattice parameter of $LiMn_2O_4$ shrinks after storage. Mn is dissolved into the electrolyte and deposited on the anode, and the surface of electrode is covered by MnO_2 after storage. The resistance and polarization of $LiMn_2O_4$/electrolyte are increased because of the covered MnO_2. Mn dissolution and the increase of Li-ion migration resistance for $LiMn_2O_4$/electrolyte surface are mainly responsible for capacity loss. The deposited MnO_2 film increases the Li-ion migration resistance of $LiMn_2O_4$/electrolyte from 20.28 to 53.31 Ω after storage, but it also separates the $LiMn_2O_4$ from electrolyte, which improves the cyclic performance.

Acknowledgements

The project was sponsored by National Basic Research Program of China (973 Program, 2007CB613607).

References

[1] A. Blyr, C. Sigala, G. Amatucci, D. Guyomard, Y. Chabre, J.M. Tarascon, J. Electrochem. Soc. 145 (1998) 194.
[2] A.D. Pasquier, A. Blyr, P. Courjal, D. Larcher, G. Amatucci, B. Gerand, J.M. Tarascon, J. Electrochem. Soc. 146 (1999) 428.
[3] Y.Y. Xia, T. Sakai, T. Fujieda, X.Q. Yang, X. Sun, Z.F. Ma, J. McBreen, M. Yoshio, J. Electrochem. Soc. 148 (2001) A723.
[4] J. Shim, R. Kostecki, T. Richardson, X. Song, K.A. Striebel, J. Power Sources 112 (2002) 222.
[5] M. Wohlfahrt-Mehrens, C. Vogler, J. Garche, J. Power Sources 127 (2004) 58.
[6] Z.S. Zheng, Z.L. Tang, Z.T. Zhang, W.C. Shen, J. Inorg. Mater. 18 (2003) 257.
[7] F.T. Quinlan, K. Sano, T. Willey, R. Vidu, K. Tasaki, P. Stroeve, Chem. Mater. 13 (2001) 4207.
[8] Y. Xia, M. Yoshio, J. Electrochem. Soc. 143 (1996) 825.
[9] S.T. Myung, S. Komaba, N. Hirosaki, N. Kumagai, Electrochem. Commun. 4 (2002) 397.
[10] S. Komaba, N. Kumagai, T. Sasaki, Y. Miki, Electrochemistry 69 (2001) 784.
[11] A. Antonini, C. Bellitto, M. Pasquali, G. Pistoia, J. Electrochem. Soc. 145 (1998) 2726.
[12] W. Lu, I. Belharouak, S.H. Park, Y.K. Sun, K. Amine, Electrochim. Acta 52 (2007) 5837.
[13] S. Komaba, K. Oikawa, S.T. Myung, N. Kumagai, T. Kamiyama, Solid State Ionics 149 (2002) 47.
[14] K. Amine, H. Tukamoto, H. Yasuda, Y. Fujita, J. Power Sources 68 (1997) 604.
[15] Y.S. Hong, C.H. Han, K. Kim, C.W. Kwon, G. Campet, J.H. Choy, Solid State Ionics 139 (2001) 75.
[16] G. Kumar, H. Schlorb, D. Rahner, Mater. Chem. Phys. 70 (2001) 117.
[17] R. Alcantara, M. Jaraba, P. Lavela, J.L. Tirado, J. Electrochem. Soc. 151 (2004) A53.
[18] C.S. Yoon, C.K. Kim, Y.K. Sun, J. Power Sources 109 (2002) 234.
[19] C. Julien, S. Ziolkiewicz, M. Lemal, M. Massot, J. Mater. Chem. 11 (2001) 1837.
[20] D. Capsoni, M. Bini, G. Chiodelli, V. Massarotti, P. Mustarelli, L. Linati; M.C. Mazzati, C.B. Azzoni, Solid State Commun. 126 (2003) 169.
[21] Y. Shin, A. Manthiram, Electrochem. Solid State Lett. 5 (2002) A55.
[22] A. Eftekhari, Solid State Ionics 167 (2004) 237.
[23] J.S. Gnanaraj, V.G. Pol, A. Gedanken, D. Aurbach, Electrochem. Commun. 5 (2003) 940.
[24] H. Yamane, M. Saitoh, M. Sano, et al., J. Electrochem. Soc. 149 (2002) 1514.
[25] K. Takahashi, M. Saitoh, N. Asakura, et al., J. Power Sources 136 (2004) 115.
[26] M. Saitoh, M. Sano, M. Fujita, et al., J. Electrochem. Soc. 151 (2004) A17.
[27] Y. Li, M. Takahashi, B.F. Wang, Electrochim. Acta 51 (2006) 3228.
[28] J. Cho, M.M. Thackeray, J. Electrochem. Soc. 146 (1999) 3577.
[29] X. Yongyao, M. Yoshio, J. Power Sources 66 (1997) 129.
[30] M.D. Levi, K. Gamolsky, D. Aurbach, et al., J. Electrochem. Soc. 147 (2000) 25.